



Subtropical Low Cloud Response to a Warmer Climate in a Superparameterized Climate Model. Part II: Column Modeling with a Cloud Resolving Model

Peter N. Blossey¹, Christopher S. Bretherton^{1,2} and Matthew C. Wyant¹

¹ Department of Atmospheric Sciences, University of Washington, Seattle, Washington, USA

² Department of Applied Mathematics, University of Washington, Seattle, Washington, USA

Manuscript submitted 19 March 2009; in final form 5 May 2009

A cloud resolving model (CRM) is used to investigate the low-cloud increase due to a 2 K SST increase in the SP-CAM superparameterized climate model. Of particular interest is the sensitivity of cloud changes to the CRM resolution (4 km horizontal, 30 vertical levels) in SP-CAM. The CRM is run in column-modeling framework using SP-CAM composite cloud regimes. The experiments are run to steady state using composite advective tendencies, winds, and sea-surface temperature from the control and +2 K climates of SP-CAM. A new weak temperature gradient algorithm based on an idealized form of gravity wave adjustment is used to adjust vertical motion in the column to keep the simulated virtual temperature profile consistent with the corresponding SP-CAM composite profile. Humidity is also slowly relaxed toward the SP-CAM composite above the boundary layer. With SP-CAM grid resolution, the CRM shows +2 K low cloud increases similar to SP-CAM. With fine grid resolution, the CRM-simulated low cloud fraction and its increase in a warmer climate are much smaller. Hence, the negative low cloud feedbacks in SP-CAM may be exaggerated by under-resolution of trade cumulus boundary layers.

DOI:10.3894/JAMES.2009.1.8

1. Introduction

Cloud resolving models (CRMs) can directly simulate turbulent cloud processes by using much finer spatial resolution than general circulation models (GCMs), but are typically run for shorter periods with much smaller domains due their heavy computational requirements. One approach to representing clouds in climate models is superparameterization, in which a CRM is embedded in each grid column of a conventional GCM.

A companion paper (Wyant et al. 2009, hereafter W09) explored the substantial low cloud increase over low-latitude oceans (LLO) simulated by a superparameterized climate model (SP-CAM, Khairoutdinov and Randall, 2001) in a climate change experiment in which the SST is uniformly raised by 2K. The model output for the control and +2K climate were sorted into cloud regimes using lower-tropospheric stability (LTS). The resulting analysis suggests that increased clear-sky radiative cooling in the moist boundary layer over the subtropical oceans is responsible for the large low cloud increase as the surface temperature is warmed.

In this paper, we use the System for Atmospheric Modeling CRM (SAM, Khairoutdinov and Randall, 2003) in a column-modeling framework as a simpler context in which to simulate these cloud changes and their relationship

to CRM resolution. This CRM is identical to the one used in SP-CAM. We will deliberately use the term ‘column modeling’ rather than ‘single-column modeling’, because as in SP-CAM, we run a CRM with prescribed large-scale advective forcings (but multiple internal grid columns) in place of a conventional GCM single-column model. This column modeling framework is similar in some respects to an idealized approach proposed by Bony et al. (2004).

Our framework is also related but not identical to those used in recent studies by Zhang and Bretherton (2008) and Caldwell and Bretherton (2008, hereafter CB08). Two key assumptions that we share with these two studies are: (a) in low latitudes, gravity waves adjust the temperature profile in each tropospheric column towards a roughly moist-adiabatic profile that is controlled remotely by deep convection over the warmest oceans, and (b) in the synoptically quiescent subtropical trades, the boundary layer cloud response to climate change is mainly due to changes in the mean state, rather than in the transient variability. Like these studies, our column methodology is applicable to

To whom correspondence should be addressed.

Peter N. Blossey, University of Washington, Atmospheric Sciences, Seattle, WA 98195-1640, USA
bloss@atmos.washington.edu

GCMs other than SP-CAM. We refine their methodology to more quantitatively match the climatology and +2K cloud response of the studied GCM in boundary-layer cloud regimes defined using specified percentile ranges of LTS. We then test how this cloud response changes with CRM horizontal and vertical resolution. This allows us to predict what CRM resolution would be required in a superparameterized GCM in order to reliably infer the response of low-latitude boundary layer clouds to a climate perturbation, which in turn is a central contributor to global cloud feedbacks on climate change.

Zhang and Bretherton (2008) examined the +2K response of subtropical stratocumulus in a single-column version of a conventional GCM, the CAM. CB08 analyzed the climate change response of a mixed-layer model of the stratocumulus-capped boundary layer. Both studies adjusted the free-tropospheric temperature toward a moist adiabat related to warm-ocean SST (with significant methodological differences), assumed a constant free-tropospheric relative humidity, and let the column model drive the boundary-layer turbulent mixing and cloud. Both models made strong simplifying assumptions about horizontal advection and they computed mean vertical velocity in the column based on a heat budget. That is, mean subsidence in each column adjusts to keep the temperature roughly anchored to the same moist adiabat. CB08 used a more sophisticated representation of these feedbacks than did Zhang and Bretherton (2008).

Each of these studies, like SP-CAM, predicted a boundary-layer cloud albedo increase (negative cloud feedback) in the warmer climate. However, the physical mechanisms were quite different, both from each other and from the radiatively-driven mechanism for low cloud increase described in W09 that appears to operate in SP-CAM. Zhang and Bretherton (2008) found that a complex and somewhat unphysical interaction between many moist physical parameterizations produces a +2K boundary-layer cloud albedo increase in the single-column version of CAM in a stratocumulus-like cloud regime. This increase is also seen in global CAM simulations, suggesting that the +2K cloud response in the global simulations may be artificial. However, both the mean state and +2K change in the boundary-layer clouds were rather different between their single-column model and the global CAM simulations of the corresponding subtropical cloud regime. Meanwhile, CB08 found that stratocumulus clouds thicken in a +2K climate due to ‘subsidence lapse-rate’ feedback, in which the inversion strengthens (suppressing dry air entrainment and lowering cloud base) and mean subsidence weakens in the warmer climate (so the cloud top can nevertheless rise). The net result is an increase in cloud thickness. Their result applies only to the small fraction of the subtropical oceans usually covered by stratocumulus-capped mixed layers. This is a regime poorly simulated in SP-CAM due to inadequate CRM resolution.

Our general approach in this paper is to use W09’s LTS-composites of the SP-CAM control and +2K experiments to provide initial conditions and forcings for column-model experiments. We compare steady-state CRM fields for the two cases to test if the control cloud cover and the +2K response are similar to the SP-CAM composited response. If so, the column analogue may provide a useful guide to tropics-wide boundary layer cloud feedbacks to climate change.

The outline of this paper is as follows: In sect. 2 we describe our CRM column analogue, and in sect. 3, we show that it can approximately simulate the mean cloud and +2K cloud response of SP-CAM composited over an LTS percentile range that corresponds to a cloud regime transitional between stratocumulus and shallow cumulus. In sect. 4, we use this column analogue to explore the sensitivity of the boundary-layer cloud response to the use of a much finer CRM grid resolution than currently used in SP-CAM. Sections 5 and 6 explore the sensitivity of the column analogue to the inclusion/exclusion of a diurnal cycle of insolation and to changes in the formulation of the column modeling approach. A discussion and our conclusions are presented in sect. 7.

2. SP-CAM column analogue — description

The analysis of SP-CAM in W09 suggests the low cloud increases are quite pervasive across the subtropical oceans. Hence, we could pick some individual LLO grid column for this test, compute mean forcings for this column, and run our column model with these forcings. To more convincingly connect the results to average trends across the entire LLO, we instead apply this approach to a composite over all LLO grid column-months in a particular climate regime.

Following W09, we use deciles of LTS to define our climate regimes. The geographic location of SP-CAM grid columns in the three deciles of highest LTS are shown in Fig. 1. For each decile, columns are shaded based on the number of months in which their LTS lies in that decile. The term LTS70-80 will refer to the decile consisting of the 70-80th percentiles of LTS, ordered from lowest to highest, and similarly for other deciles. The LTS70-80 locations lie mainly in the trade cumulus belts to the north and south of the equator. The great majority of the LTS90-100 locations sit off the western coasts of continents in the subtropics, in areas where stratocumulus decks are commonly observed. The LTS80-90 locations lie mainly in the climatological transitions between stratocumulus and trade cumulus clouds.

For our column modeling, we focus primarily on the 80-90 percentile of LTS (hereafter LTS80-90) analyzed in W09, which has strong +2K low cloud increases, minimal cirrus, and no coastal fog. Results are also considered for the 70th-80th percentile of LTS (LTS70-80) to explore the performance of the column analogue to changes in forcing. As discussed in W09, the SP-CAM simulated a lot of spurious

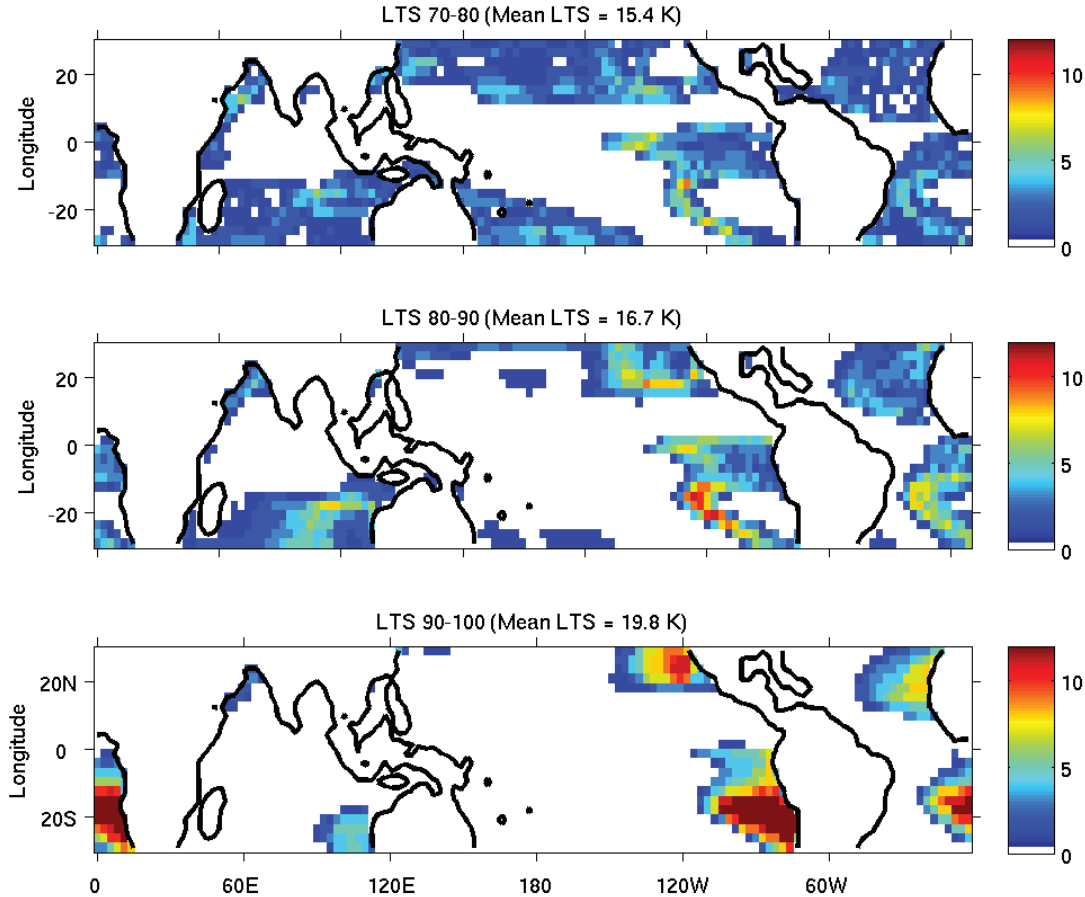


Figure 1. Geographic location of SP-CAM grid columns within top three LTS bins: 70th-80th, 80th-90th and 90th-100th percentiles. Colors indicate number of months in a given LTS bin per year.

fog in the LTS90-100 regime, and an accurate large-eddy simulation (LES) of the stratocumulus typical of the LTS90-100 regime typically requires very high vertical resolution of 10 m or less (Stevens et al. 2005). Because of this, we defer column-modeling of the LTS90-100 regime to a future paper in which these issues can be better addressed.

We run the CRM to steady state with the composite forcings for the control climate (CTRL) and repeat for the +2K climate. Let C be a key summary cloud statistic (e. g. low cloud cover or shortwave cloud forcing, SWCF), with value C_{CRM} in the control-forced CRM and value C_{GCM} in the control GCM composite. Let the difference in C between the two CRM simulations be $\Delta C_{CRM} = C_{CRM}^{+2K} - C_{CRM}$. If C_{CRM} is comparable to C_{GCM} and ΔC_{CRM} is comparable to ΔC_{GCM} then the column analogue has skill and further analysis of its low cloud sensitivity of the single column model to the +2K forcing change is warranted. Otherwise, the time averaging and LTS-compositing has removed essential ingredients of the +2K low cloud changes.

2.1. CRM configuration and boundary conditions

We configure the SAM CRM to use the same algorithms as in SP-CAM for microphysics, radiation, surface fluxes. The sea surface temperature (SST) is taken from the SP-CAM LTS composite, and the diurnal cycle of insolation is specified so that the mean insolation matches that of the SP-CAM LTS composite. Note that the LTS80-90 and LTS70-80 runs use 22°N and 18°N latitude, respectively, for the computation of insolation and the Coriolis force.

The two-dimensional configurations of domain and resolution for the CRM used in the present study are listed in Table 1. The $\Delta x = 4$ km or ‘CRM4km’ configuration matches the SP-CAM CRM in domain size and resolution. To establish whether the CRM configuration used in SP-CAM has adequate resolution to examine the low cloud response, and if not, what resolution would suffice, we also consider ‘LES’ configurations of the same CRM. These have much finer grid spacings in the lower troposphere of 50–400m in the horizontal and 20–160 m in the vertical, along

Table 1. CRM configuration parameters

Configuration	Domain size (km)		Grid spacing (m)		Grid points	
	x	z	Δx	Δz below 3.5 km	x	z
CRM4km	128	40	4000	132-922	32	30
LES400	51.2	27	400	160	128	64
LES200	51.2	27	200	80	256	96
LES100	51.2	27	100	40	512	160
LES50	51.2	27	50	20	1024	288

with a shorter domain length of 51.2 km. The vertical grid is stretched starting at approximately 3.5 km, and Δz reaches 1 km at the domain top. These grid spacings were chosen to bracket those used in Siebesma et al. (2003)'s intercomparison of nonprecipitating trade cumulus convection ($\Delta x = 100$ m, $\Delta z = 40$ m), which showed little sensitivity of the simulated cloud statistics to choice of LES model or further increases in resolution. A full suite of three-dimensional simulations was too computationally expensive for the long integrations performed here. However, a five-day-long three-dimensional LES run at the same resolution as the LES50 simulations indicated that the sensitivity of short-wave cloud forcing to dimensionality was much smaller than its sensitivity to resolution.

An idealized vertical profile of winds is constructed for the CRM simulations (Fig. 2). The horizontal velocity components are not directly composited because this would produce unrealistically weak wind speed and vertical shear. Instead the monthly-mean wind speed (which includes rectification from transients) is composited at each level. An idealized profile of wind directions, based on the RICO wind profile used by Abel and Shipway (2007), is combined with the composite wind speed profiles to create u (E-W) and v (N-S) velocity profiles. These are used to initialize the

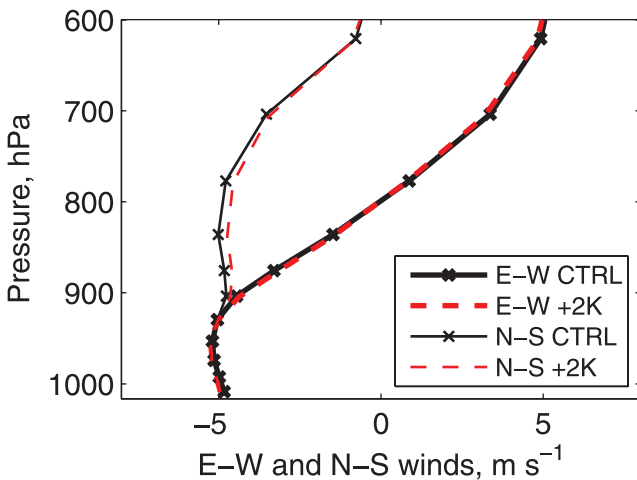


Figure 2. Wind profiles used to force the CRM. u (E-W, thick) and v (N-S, thin) wind profiles (m s^{-1}) for the control (black) and +2K SST (red) cases are derived from the LTS80-90 composite wind speed profile and the RICO wind direction profile. SP-CAM vertical grid levels are shown with the 'x' symbols.

runs and to nudge their domain-mean velocity profiles with a 10-minute timescale. This timescale is chosen to keep the surface winds close to the bin-mean values from SP-CAM, so that the surface fluxes will be consistent with those in SP-CAM if the near-surface air properties are similar. The CRM domain is oriented N-S, as in SP-CAM. The results are somewhat dependent on this choice for the orientation of the domain because only the shear component along the horizontal domain axis affects the simulation. This would not be the case for three-dimensional simulations.

2.2. CRM initialization and advective forcing

The CRM experiments are initialized with the SP-CAM LTS80-90 composite profiles of temperature and moisture (Fig. 3, thin lines) with small-amplitude white noise in temperature added to initiate convection. The steady state reached depends on how the model is forced. This requires one to make choices about the specification of advective forcings, wind direction, and nudging. Unlike the prior studies discussed in the introduction, we advectively force and nudge the mean state toward the SP-CAM thermodynamic profiles rather than a moist adiabat, so that our column simulation creates a cloud environment similar to the LTS80-90 composite. We force the CRM with the LTS80-90 composite of the SP-CAM large-scale horizontal advective tendencies and vertical pressure-velocity (the advective tendencies are plotted in Fig. 10 in W09). The composite vertical velocity from SP-CAM is plotted in Fig. 4 (thin lines). When forcing the CRM, this vertical velocity is adjusted (thick lines) using a method that we will now describe.

In SP-CAM, the composite diabatic heating and moistening rates closely balance the sum of the resulting horizontal and vertical advective tendencies. However, the CRM diabatic tendencies inevitably will not exactly balance the SP-CAM composite advective tendencies, so the CRM mean profiles start to drift away from the SP-CAM profiles to which they are initialized. Slow but persistent drifts in the free troposphere must be controlled so that the simulated boundary layer evolves under free-tropospheric profiles that remain close to the SP-CAM composite. For instance, the SP-CAM composite has slight advective moistening in the upper troposphere to balance drying from ice precipitating out of occasional high cirrus, even though the composite sounding is not ice-saturated at upper levels. This advective moistening slowly moistens the CRM simulation in the

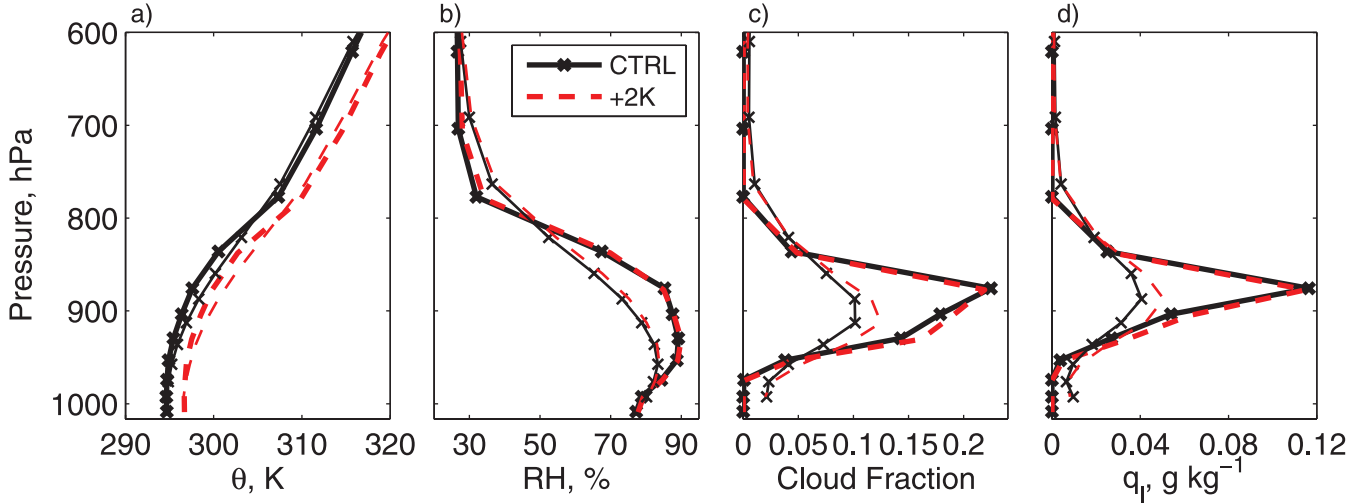


Figure 3. Vertical profiles from SP-CAM LTS80-90 composite (thin) and the horizontal and time mean profiles from CRM4km runs (thick). (a) potential temperature (K), (b) relative humidity (%), (c) cloud fraction and (d) cloud liquid water content (g kg^{-1}).

upper troposphere. If uncompensated, this drift would ultimately lead to an unrealistic sheet of thin cirrus near the tropopause.

The scheme used to control these drifts affects the +2K sensitivity of the results. We first tried a simple approach, which is to relax the temperature and humidity profiles toward their LTS80-90 values with a time constant that is short in the free troposphere and long below the trade inversion. We retained this approach for humidity (see next section) but not for temperature.

2.3. CRM moisture nudging

Systematic drift of the upper-tropospheric humidity from the reference profile is an inevitable consequence of using a

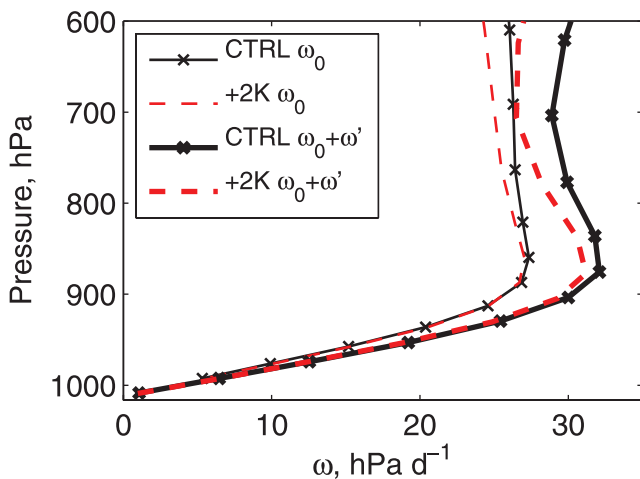


Figure 4. SP-CAM composite pressure velocity (ω_0 , thin) and adjusted pressure velocity ($\omega_0 + \omega'$, thick, hPa d^{-1}) used to force the CRM. Black lines represent the control and red lines the +2K climate.

quasi-steady CRM simulation to represent a composite over many times and locations. Hence, we add a relaxation term for specific humidity with a height dependent rate

$$a_q(z) = a_{ft} \{1 + \text{erf}[(z - z_0)/b]\}/2, \quad (2.1)$$

where $a_{ft} = (1 \text{ d})^{-1}$, $z_0 = 3 \text{ km}$, and $b = 1.5 \text{ km}$. This nudging rate ramps from close to zero at the surface to a_{ft} in the upper troposphere, with the transition mainly occurring just above the trade inversion in the height range $z_0 \pm 2b/3 = 3 \pm 1 \text{ km}$.

2.4. Vertical velocity feedback for the CRM

Our approach for controlling temperature drifts from the reference profile invokes the same physics that underlie the ‘weak temperature gradient’ (WTG) approximation to tropical dynamics (Sobel and Bretherton 2000). This approximation assumes that the nonlocal horizontal homogenization of the temperature profile in the tropics occurs via stratified adjustment, so that the column mean vertical motion adjusts to compensate changes in the column profiles of diabatic heating. This feedback was implemented using the following adaptation of an algorithm from CB08. Let subscript ‘0’ denote a reference profile (in our case, from the SP-CAM LTS80-90 composite), and let a prime denote a perturbation of a CRM horizontal mean quantity from that reference profile. We use the reference horizontal advective tendencies, but we let the mean vertical velocity used to compute vertical advective tendencies respond to the instantaneous profile of column virtual temperature (i. e. density) anomalies. That is, we take $\omega = \omega_0 + \omega'$, where $\omega_0(p)$ is the SP-CAM reference profile and $\omega'(p, t)$ is a diagnosed time-dependent pressure velocity perturbation.

Following CB08, the approach is to consider the column to be representative of the center of an anomalous region of

some half-width Λ . The density profile across this region is assumed to have a horizontally sinusoidal variation with wavenumber $k = \pi/(2\Lambda)$ such that the density anomaly vanishes at a distance Λ from the column. We compute ω' from the linear, quasi-steady, damped inertia-gravity-wave adjustment of this horizontally-varying density field to the reference density profile. The tropopause and surface are approximated as rigid boundaries. We assume a Rayleigh damping rate a_m for momentum perturbations. This results in the following boundary-value problem, derived in Appendix A, which is solved at each timestep for $\omega'(p)$:

$$\frac{\partial}{\partial p} \left(\frac{f^2 + a_m^2}{a_m} \frac{\partial \omega'}{\partial p} \right) = \frac{k^2 R_d T_v'}{p} \quad (2.2)$$

with $\omega'(p_S) = \omega'(p_T) = 0$

Here f is the Coriolis parameter, and $p_S = 1016$ hPa and $p_T \sim 100$ hPa are the surface and tropopause pressure, respectively. We choose a momentum damping rate $a_m(p) = 1 \text{ d}^{-1} (p/p_{ref})$ where $p_{ref} = 1000$ hPa. This is largest in the lower troposphere and falls off with height, as one would expect in the subtropics where a dearth of deep convection would allow momentum anomalies in the upper troposphere to be longer lived. We also somewhat arbitrarily choose $k = 2.4 \times 10^{-6} \text{ m}^{-1}$, corresponding to a half-width $\Lambda = 650$ km for the cloud regime we are considering. The Appendix further discusses the choice of constants and the relation of this approach to published alternatives of Raymond and Zeng (2005), CB08 and Kuang (2008).

We also tried nudging the temperature to its reference profile with a damping rate profile similar to (2.1) to control temperature drift with respect to the SP-CAM sounding. This approach gives LTS80-90 simulated boundary layer cloud and +2K response that are fairly similar to those we obtain using the ω -feedback approach described above that we ended up adopting. In corresponding LTS70-80 simulations, temperature nudging is less successful than ω -feedback in reproducing the SP-CAM +2K cloud changes, though both methods replicate the control-state clouds fairly well. In general, the ω -feedback approach also produces a somewhat better match than temperature nudging between the CRM-simulated cloud-layer relative humidity profile and the SP-CAM composite.

3. SP-CAM column analogue - CRM4km results

Each simulation reaches statistically-steady horizontal-mean temperature and moisture profiles within 20 days. Low cloud fraction (not shown) adjusts even more rapidly. However, while successive daily means of low cloud fraction and of shortwave cloud forcing (SWCF)¹ are uncorrelated, low frequency variability is present, as seen in the timeseries of ten-day-averaged SWCF in Fig. 5a. Because we are interested in the differences between two rather similar simulations, we must be sure to use a sufficiently long

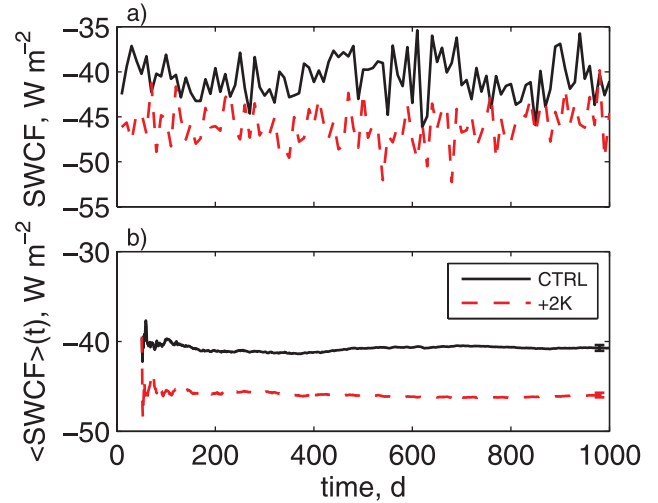


Figure 5. Time series of (a) ten-day-averaged shortwave cloud forcing (SWCF) and (b) $\langle \text{SWCF} \rangle(t)$, the average of SWCF over days 51 up to t , for CRM4km runs. Control (black, solid) and +2K (red, dashed) runs are shown. Standard error estimates for time-averaged SWCF are shown just inside the right edge of (b).

averaging period so their differences overwhelm the sampling uncertainty in this and other cloud-related variables. As a result, we choose an averaging time of 950 days (from days 50–1000) for CRM4km to reduce uncertainty in the time averages caused by the low frequency variability. Figure 5b shows the evolution of $\langle \text{SWCF} \rangle(t)$, the average SWCF between day 50 and day t , and indicates that the time-average is well converged over the time period considered here. Time averages for the LES simulations, which lack significant low frequency variability, are taken over days 50–100 (except for $\Delta x=400\text{m}$, which uses days 50–200). Standard error estimates for all runs are generated from ten sample means over ten equal length subperiods of the full averaging period (e.g., 950 days for CRM4km). These are shown for the CRM4km runs at the right edge of Fig. 5b. Standard error estimates for ΔSWCF are computed from the sums of the squares of the error estimates for the individual control and +2K runs.

Figure 3 (thick lines) shows the steady-state horizontal-mean profiles of potential temperature, relative humidity, cloud fraction, and liquid water content reached by the LTS80-90 forced control and +2K CRM4km runs. The CRM4km temperature and relative humidity profiles above the boundary layer match the SP-CAM composites fairly closely because of the vertical velocity feedback and strong moisture nudging, along with the relatively slight imbalance between CRM advective and diabatic forcings at these levels.

¹ $\text{SWCF} = \text{SW}_{\text{dn}}^{\text{net}} - \text{SW}_{\text{dn}}^{\text{clr}}$, where $\text{SW}_{\text{dn}}^{\text{net}}$ and $\text{SW}_{\text{dn}}^{\text{clr}}$ are the net downwelling shortwave radiation flux at the top of the atmosphere for full-sky and clear sky, respectively. Longwave cloud forcing (LWCF) is defined similarly. As the effect of low clouds on LWCF is weak (see table 2) due to cloud top temperatures not so different from those of the surface, shortwave cloud forcing represents the main contribution of low clouds to climate sensitivity.

Table 2. Comparison of SP-CAM, CRM4km and LES100 summary statistics for the control runs and the +2K change. The composite control SST's are 297.1 K and 298.2 K for LTS80-90 and LTS70-80, respectively.

Case	Model		Low Cloud Fraction	LWP (g m ⁻²)	SWCF (W m ⁻²)	LWCF (W m ⁻²)	Surf. Evap. (mm d ⁻¹)	Rainfall (mm d ⁻¹)
LTS80-90	SP-CAM	ctrl	0.28	54.7	-45.5	11.2	4.49	0.67
		Δ_{+2K}	0.05	8.0	-5.4	0.2	0.47	0.05
	CRM4km	ctrl	0.34	86.9	-40.7	5.3	4.43	0.39
		Δ_{+2K}	0.02	5.2	-4.3	-0.3	0.46	0.06
	LES100	ctrl	0.09	16.4	-10.8	2.0	4.39	0.21
		Δ_{+2K}	0.01	1.5	-0.9	0.1	0.51	0.02
LTS70-80	SP-CAM	ctrl	0.27	59.2	-44.5	14.1	4.95	1.33
		Δ_{+2K}	0.02	5.0	-3.4	-0.4	0.48	0.05
	CRM4km	ctrl	0.36	90.2	-45.6	5.9	4.87	0.46
		Δ_{+2K}	0.01	3.2	-0.9	-0.5	0.45	0.04
	LES100	ctrl	0.09	18.7	-11.6	1.9	4.81	0.41
		Δ_{+2K}	0.00	0.2	-0.2	0.0	0.49	-0.01

The CRM deviates more from the SP-CAM composite profiles in the boundary-layer cloud layer. The cool, moist boundary layer is deeper and capped by a more pronounced inversion in CRM4km than in SP-CAM. We speculate that this occurs because, in SP-CAM, synoptic transients episodically depress the trade inversion and replace moist cool air by warmer and drier air. By construction, this cannot occur in the steadily forced CRM.

Nevertheless, the SWCF and its +2K sensitivity agree fairly well between CRM4km and SP-CAM. The low cloud fraction and liquid water path (LWP) of the CRM4km runs increase from control to +2K as in SP-CAM, though the changes are smaller in magnitude than in SP-CAM. Table 2 summarizes time-averaged statistics of the CRM4km and LES100 runs for both the control and the +2K changes. The means and +2K sensitivities of low cloud fraction, cloud liquid water path and SWCF show reasonable agreement between CRM4km and SP-CAM. Table 2 also shows corresponding results for the CRM run with LTS70-80 forcing, which show similar agreement with SP-CAM, except that the +2K sensitivity of SWCF is somewhat smaller in magnitude than in SP-CAM. Overall, we regard the CRM4km simulation as a useful column analogy to the SP-CAM composite cloud response.

Table 2 also shows that the control SP-CAM composite rainfall rate is about 70% larger than in CRM4km for LTS80-90 and 190% larger for LTS70-80. This is because the SP-CAM composites include occasional episodes of deeper convection as well as the light shallow convective rainfall simulated by the CRM. The heating and drying from these episodes affect the SP-CAM composite heat and moisture budgets. However, in both cases the precipitation is much smaller than evaporation from the sea surface, and similarly for its +2K changes. Hence, the episodic precipitating deep convection does not appear to be seriously perturbing the shallow cumulus layer heat and moisture budgets and their +2K response. This is consistent with the similarity in the SP-CAM +2K cloud response across the high LTS percentiles, despite substantial differences in their mean precipitation rate.

Figure 6 shows time-averaged profiles of radiative heating, large-scale vertical advection and moisture nudging from the CRM4km simulations. The mean control radiative cooling (Fig. 6a, thick black line) is enhanced compared to SP-CAM (thin black line) in the 850–900 hPa layer in both the control and +2K simulations because of higher RH and cloud. The +2K CRM4km simulation has slightly stronger +2K radiative cooling in the cloud layer than the control, though the increase is much less than that of the SP-CAM. The control vertical advective temperature tendency (Fig. 6b) compensates for most of the radiative cooling. Subsidence drying (Fig. 6c) balances upward convective and turbulent moisture transport. Within the cumulus layer (below 800hPa), the moisture nudging (Fig. 6d) is much weaker than the vertical (Fig. 6c) and horizontal (W09 Fig. 10c) moisture advection and also shows little +2K sensitivity. We infer that the moisture nudging does not seriously distort the cloud-formation processes in the cumulus layer. Above the cumulus layer, the nudging acts to moisten the 700–800 hPa layer where the CRM does not generate as much cumulus-induced moistening as does SP-CAM (again probably due to the lack of synoptic variability that can produce somewhat deeper cumuli). Overall, the physics of the CRM4km +2K response seems similar to that diagnosed for SP-CAM as a whole: more radiative cooling leads to more shallow convection and associated cloud.

4. Sensitivity to CRM resolution

The column analogue is now employed to study the sensitivity of the SP-CAM cloud climatology and +2K response to the CRM resolution. To do this, we ran the cloud-resolving model to steady state using the same LTS80-90 control and perturbed forcing, but with the ‘LES’ resolutions given in Table 1. Figure 7 shows steady state profiles from the LES100 simulations with LTS80-90 control and +2K forcings (thick lines). Results at this resolution are representative of those at the finer LES resolutions $\Delta x=50$ –200m. The LES simulations have a sharper inversion than CRM4km and also have an increase in humidity, cloud

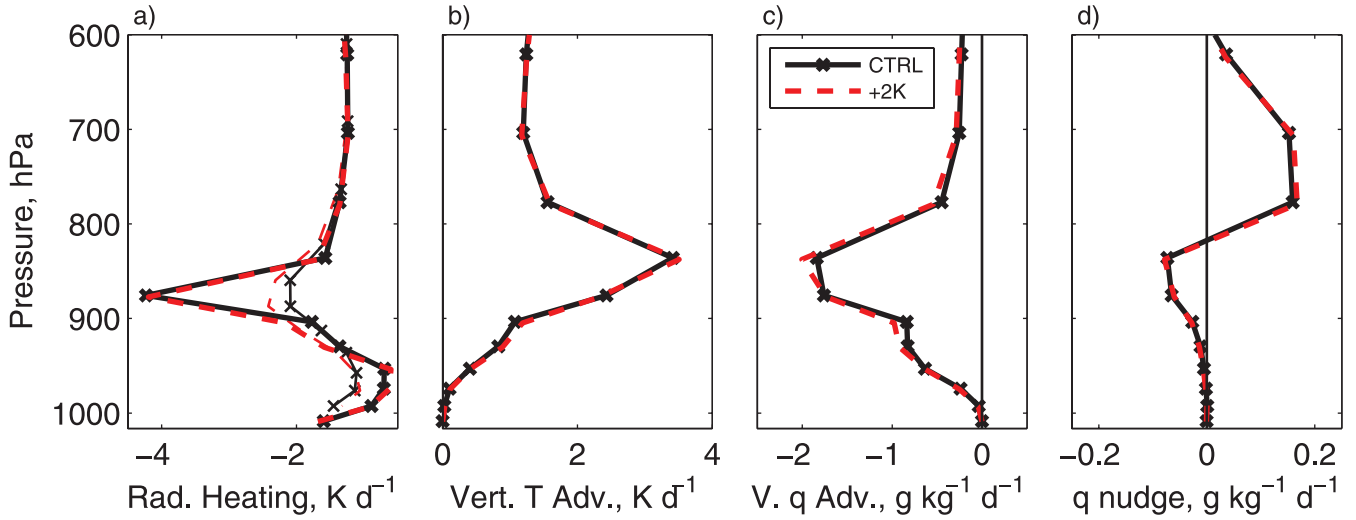


Figure 6. Horizontally- and time-averaged profiles from the CRM4km run. (a) Radiative heating (K d^{-1}), with thin lines denoting comparison SP-CAM profiles, (b)-(c) tendencies of temperature (K d^{-1}) and humidity ($\text{g kg}^{-1} \text{d}^{-1}$) from perturbation vertical advection, and (d) moisture relaxation tendency ($\text{g kg}^{-1} \text{d}^{-1}$).

cover and condensate below the inversion that is suggestive of a tendency towards cumulus-under-stratocumulus, that is not present in CRM4km. Furthermore, Figs. 7c–d show that LES100 has much less cloud and condensate at all heights, producing a low cloud fraction and SWCF only one-fourth as large as for the CRM4km resolution (see table 2). Similar results (not shown) were found with LTS70-80 forcings, but the LES cloud and condensate profiles were more weighted toward the bottom of the cloud layer, indicating that less residual cloud was present at the trade inversion base.

Given the differences in simulated mean state, it is no surprise that the +2K cloud response in the LES simulations also differs considerably from the CRM4km simulations. For the LTS80-90 case, the LES-predicted +2K response in

low cloud fraction and SWCF (Fig. 7a and Table 2, respectively) is smaller than that of the CRM4km simulation. Moreover, its vertical structure is different than the CRM4km simulation, with the cloud increase localized in the layer below the inversion.

For the LTS70-80 case the LES-predicted cloud and condensate (not shown) also increase near the trade inversion in the +2K simulations, but the increase is much smaller, so that the SWCF (given in Table 2) is only slightly larger than in the control run and the change in the low cloud cover is negligible. Both SP-CAM and the CRM4km runs in this bin show weaker +2K cloud changes than in the LTS80-90 bin, although both of them have significantly negative +2K changes in SWCF, as was the case for LTS80-90. The +2K change in SWCF in SP-CAM is about

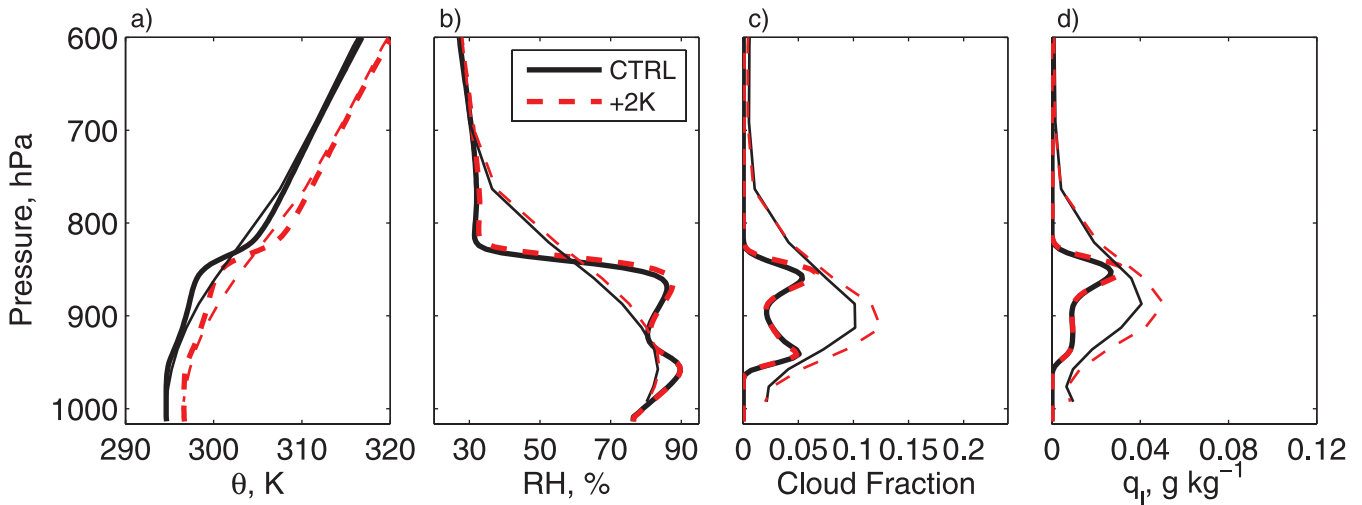


Figure 7. As in Fig. 3, except for LES100 simulations. Thin lines show SP-CAM composite values.

four times stronger than in the CRM4km runs, indicating that our column analogue is less successful in this case. We would speculate that synoptic variability may play a more important role in establishing the mean state and in determining the climate sensitivity in this bin than in the LTS80-90 bin.

The CRM4km cloud biases can be rationalized as follows. The coarse, 4 km horizontal resolution forces cumulus updrafts to be far too broad and weak. Updrafts that are too weak must have an excessive fractional area at cloud base in order to flux enough moisture out of the boundary layer to balance surface evaporation. This causes the coarse-resolution simulation to overestimate cloud fraction just above cloud base. On the other hand, cumulus updrafts that are too weak are insufficiently penetrative when they overshoot their level of neutral buoyancy. This keeps the cumulus layer too shallow. In addition, the vertical resolution is very coarse, especially at heights above 2 km.

In Figure 8, the change in SWCF and Δ SWCF with grid spacing Δx are depicted. Here, the full suite of resolutions ($\Delta x=50\text{m}$, 100m , 200m , 400m and 4km) are shown (heavy blue line). In addition, the SP-CAM results (black circles) and a number of sensitivity studies that will be described further in sect. 5 and 6 are also displayed. In both the LTS70-80 and LTS80-90 bins, the LES results show consistency in SWCF and Δ SWCF across the range $\Delta x=50\text{--}200\text{m}$ with $\Delta z=20\text{--}80\text{m}$. The discrepancy between Δ SWCF in those simulations is close to the error estimates. At the coarser grid spacing of $\Delta x=400\text{m}$ and $\Delta z=160\text{m}$, however, the amplitude of SWCF and Δ SWCF increase substantially. The SWCF increases further at the $\Delta x=4\text{km}$ resolution of CRM4km and SP-CAM, as does Δ SWCF in the LTS80-90 bin. In the LTS70-80 bin, Δ SWCF is close to the LES

estimate, even through the control SWCF is approximately four times larger than that of the LES runs.

The simulations presented in Figure 8 suggest that a grid resolution of approximately $\Delta x=250\text{m}$ and $\Delta z=100\text{m}$ is necessary to simulate the trade cumulus clouds characteristic of the LTS70-80 and LTS80-90 bins. This estimate is consistent with the notion that one should resolve at least the largest of the eddies in the $\sim 500\text{m}$ deep subcloud layer. The SWCF of a further test using $\Delta x=400\text{m}$ and $\Delta z=80\text{m}$ (not shown, identical to LES400 except that the vertical grid of LES200 was used) was between that of LES200 and LES400. This indicates that both horizontal and vertical resolution play a role in the differences between LES200 and LES400 and that the coupling of a coarse horizontal grid to a relatively fine vertical grid may not lead to satisfactory simulations of clouds in this regime.

Within the column analogue, the mean cloud state and +2K sensitivity depends on other aspects of the simulation setup, in addition to grid resolution within the CRM or LES model. In the following sections, we explore two aspects of the setup: the use of steady, diurnally-averaged insolation (rather than the default, diurnally-varying insolation) and variations in the formulation of the stratified adjustment mechanism underlying the vertical velocity feedback.

5. Sensitivity to inclusion of diurnal cycle of insolation

The CRM4km simulations have also been performed with diurnally-averaged insolation, in addition to the default, diurnally-varying insolation in the other simulations described here. While the mean liquid water path and cloud fraction change little with the inclusion or exclusion of a diurnal cycle of insolation (fig 9 shows results for LTS80-90

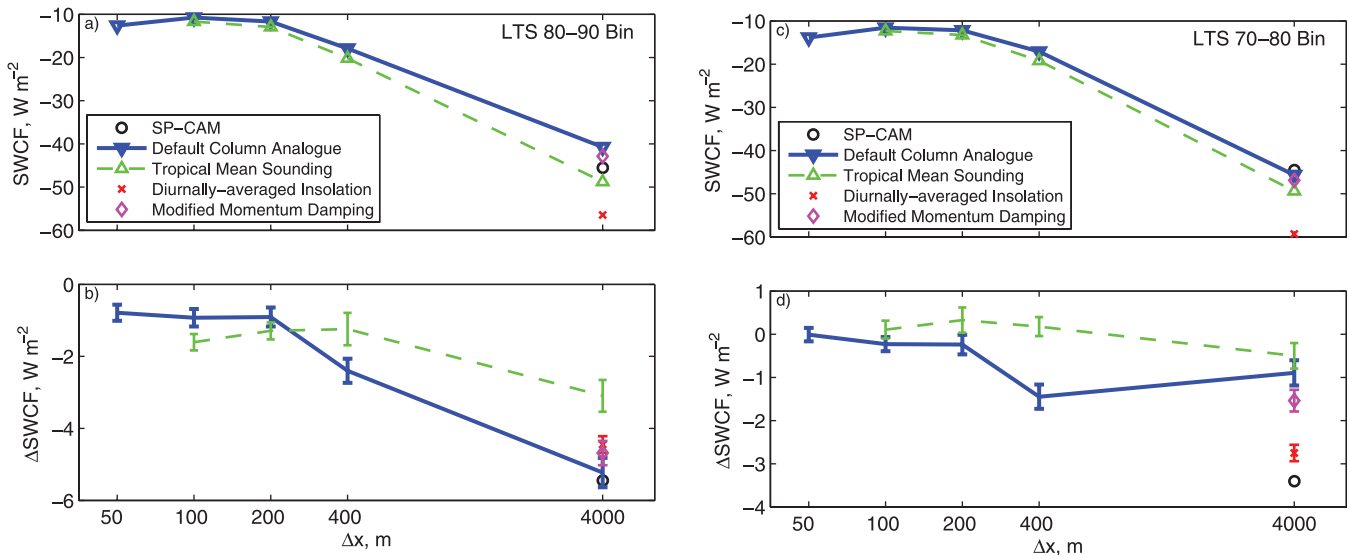


Figure 8. Plots of Δx vs SWCF and Δ SWCF for (a,b) LTS80-90 and (c,d) LTS70-80 bins. Standard error estimates for Δ SWCF are shown in (b) and (d). The scales on the horizontal axes is logarithmic in Δx . The various CRM simulations are described in the text.

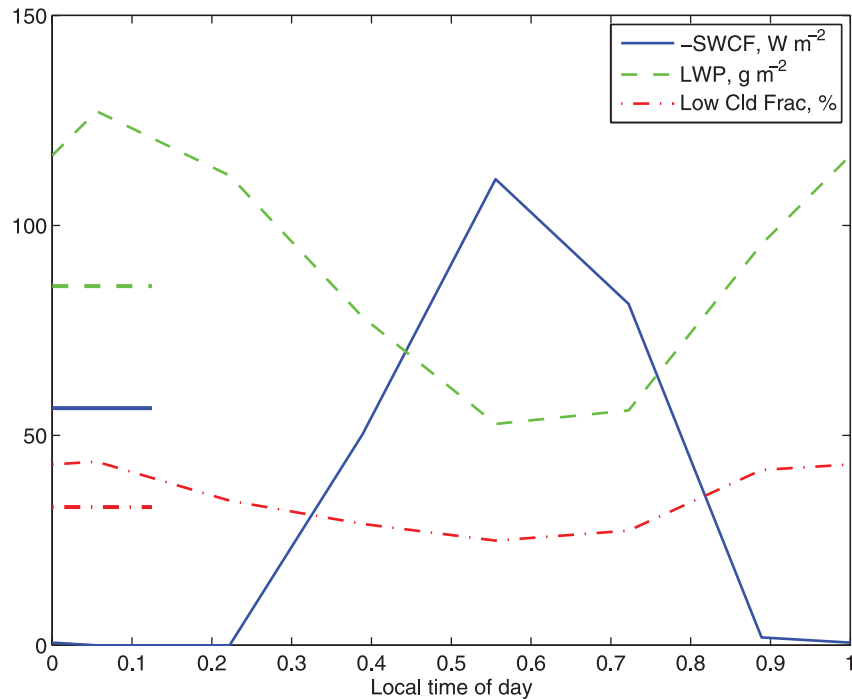


Figure 9. Diurnal cycle of -SWCF, LWP and percent low cloud fraction for CRM4km run with LTS80-90 control forcings. Also plotted with thick lines at left are mean values of the same quantities from a run that is identically-configured run except for the use of diurnally-averaged insolation.

control forcings), the SWCF increases substantially in the case of diurnally-averaged insolation. As seen in Figure 9, the cloud layer thins during the day and thickens at night with diurnally-varying insolation. Thinner cloud layers during the hours of strongest insolation lead to lower average SWCF than that found using diurnally-averaged insolation. In the LTS70-80 bin, Δ SWCF increases substantially when diurnally-averaged insolation is used (Figure 8d). This is not true in the LTS80-90 bin, where Δ SWCF is larger with diurnally-varying insolation, despite the weaker mean SWCF in that case (Figure 8a–b).

6. Sensitivity to parameterization of stratified adjustment

The vertical velocity feedback described in sect. 2.4 is central to our column analogue approach for diagnosing cloud feedbacks. Without this feedback, the CRM or LES runs would drift from the large-scale conditions derived from SP-CAM, and large or inconsistent drifts in control and +2K simulations would lead to meaningless predictions of Δ_{+2K} cloud changes. In the present section, the sensitivities of our results to changes in the the formulation of the vertical velocity feedback are explored. In this context, it can be noted that the application of the column modeling approach to both the LTS70-80 and LTS80-90 bins has already explored the sensitivity of the formulation to varying large-scale conditions. While the conditions in these bins are

broadly similar, the relatively good agreement between the CRM4km and SP-CAM results in these two bins suggests that the column analogue framework is robust with respect to small changes in the large-scale conditions.

6.1. Momentum damping

The formulation of stratified adjustment in the present work requires the specification of the vertical profile of momentum damping. Momentum damping is itself a parameterization of the role played by turbulent eddies and gravity waves in momentum transport. As it depends on the state of boundary layer and free troposphere, its value is relatively difficult to constrain *a priori*. Nonetheless, estimates do exist for regions of deep convection in the tropics (e.g., Lin et al. 2005). In the CRM4km runs, $a_m(p) = 1 \text{ d}^{-1} (p/p_{ref})$, where $p_{ref} = 1000 \text{ hPa}$, was used. An indirect estimate of momentum damping generated from SP-CAM (see appendix) suggests that a vertically-uniform momentum damping rate $a_m = 0.5 \text{ d}^{-1}$, along with $\Lambda = 650 \text{ km}$, would also be consistent with SP-CAM. Simulations identical to CRM4km except for this choice of a vertically-uniform $a_m = 0.5 \text{ d}^{-1}$ have been performed and are shown in figure 8 (magenta diamonds). The mean SWCF in these simulations is similar to that of CRM4km in both LTS bins, suggesting that the simulation of the mean state cloud forcing is relatively insensitive to this variation in the specification of a_m . The differences in Δ SWCF between the bins are larger

in relative terms and change sign between the bins. The error bars for ΔSWCF based on the standard error estimates, however, are nearly overlapping for these runs.

6.2. Tropical mean reference state

In this section, we describe how the column model can use a tropical-mean temperature profile as its reference state, together with local SST, wind speed and profiles of RH and horizontal advective forcings. In this approach, the entire ω profile is diagnosed rather than just perturbed from the LTS80-90 reference ω profile. The success of this approach suggests that the LTS80-90 ω profile and its response to a +2K SST change can be regarded as diabatically driven consequences of the local column diabatic heating profile. This further implies that $\omega(p)$ can be treated as a response rather than a forcing for the boundary layer cloud feedback problems.

Formally, an assumption underlying the derivation of the vertical velocity feedback in (2.2) is the existence of a quasi-steady reference state, that varies on timescales much longer than those of the stratified adjustment modeled in (2.2). In the runs described above, the reference state was derived from the bin-averaged soundings and profiles of large-scale horizontal advection and ω_0^{bin} , where the superscript *bin* refers to value in the LTS70-80 or LTS80-90 bin. In that framework, the vertical velocity feedback determined the perturbation large-scale vertical velocity ω' based on the deviation $T_v' = T_v - T_v^{bin}$. One could also interpret the reference large-scale vertical velocity ω_0^{bin} as that induced by a virtual temperature anomaly $T_v' = T_v^{bin} - T_v^{tropics}$ where $T_v^{tropics}$ is the tropics-mean virtual temperature profile. This interpretation, in fact, is used to derive the indirect, SP-CAM-based estimate of momentum damping in the appendix.

This approach has been extended to the column analogue by choosing the SP-CAM tropical mean sounding from the control and +2K simulations as the reference state with the reference large-scale vertical velocity $\omega_0^{tropics}=0$. Using this approach, (2.2) is used to predict the full value of ω based on the virtual temperature anomalies $T_v' = T_v - T_v^{tropics}$. Values of SWCF and ΔSWCF from simulations using this approach at the CRM and a variety of LES resolutions are reported in figure 8 (green dashed line marked ‘‘Tropical Mean Sounding’’). The trade inversion capping the cloud layer is slightly deeper in these runs (not shown) than in those using the bin-specific LTS70-80 and LTS80-90 reference state, which leads to slightly stronger SWCF in these runs. The trend in SWCF with grid spacing is much the same as reported in sect. 4. The cloud response ΔSWCF in these runs is similar to those reported above at LES resolutions up to 200m, although the standard error estimates do not always overlap. At larger grid spacings, the predicted ΔSWCF is somewhat weaker than that predicted with the bin-specific reference state, but still has the same tendency to be significantly more negative than the high-resolution LES cases.

7. Discussion and conclusions

This study further analyzes the low-latitude cloud response of SP-CAM to a uniform +2K SST increase. We use LTS-composited SP-CAM monthly-mean output of oceanic low-latitude grid columns from W09 for both control and +2K climates. A column analogue to SP-CAM is constructed and compared with the SP-CAM in two trade cumulus regimes defined by the 70-80th and 80-90th percentiles of LTS. It uses a single CRM interacting with a free troposphere in which subsidence is allowed to adjust to the column diabatic cooling to keep the temperature profile close to the SP-CAM composite, with additional humidity relaxation above the cumulus layer.

Especially for LTS80-90, the column analogue produces an encouragingly similar cloud climatology and +2K cloud response to SP-CAM when the CRM is run with the same coarse 4 km, 30 level resolution. However, the mean cloudiness dramatically decreases in this column analogue if the CRM is instead run with a typical LES resolution used for shallow cumuli.

The +2K cloud increase also is reduced at LES resolutions, as compared to the 4 km CRM resolution. Unlike with coarse resolution, cloud increases at the LES resolutions occur almost exclusively at the trade inversion. This suggests that, at LES resolution, the +2 K cloud increase may best be interpreted mainly as a consequence of the stronger trade inversion. As seen in Fig. 7, the cumuli have very similar properties in the control and +2K simulations as they rise toward the inversion, but within 100 m of the inversion, the cloud fraction and liquid water content are about 25% larger in the +2K simulations. This suggests that the condensate detrained from cumuli can survive longer under the stronger +2K inversion, consistent with past modeling studies on the stratocumulus to trade cumulus transition (e.g., Wyant et al. 1997). The inversion also seems to deepen very slightly in the +2K case, but this does not play an obvious role in the cloud increase.

While the results presented here suggest that under-resolution of cumulus clouds in the embedded CRMs within SP-CAM leads to an over-prediction of cloud fraction and cloud forcing in the LTS70-80 and LTS80-90 bin, past experience suggests that the same under-resolution likely leads to an underprediction of cloud fraction in the LTS90-100 bin. Stevens et al. (2002) found increasing stratocumulus cloud fraction with decreasing grid spacing in nighttime simulations of cumulus-under-stratocumulus with strong subsidence (nearly twice as strong as here). Similarly, Stevens et al. (2005) found increasing cloud liquid water path in simulations of stratocumulus with increasing vertical resolution (down to $\Delta z=1\text{m}$). The difficulty of achieving convergence in large eddy simulations of stratocumulus clouds — even at relatively fine resolutions — was one reason why the LTS70-80 and LTS80-90 were chosen as the focus of this first study with the column modeling approach. In the future, we plan to apply this

column modeling approach to both stratocumulus (as in the LTS90-100 bin) and the deep convection that occurs in the lower LTS bins.

A practical modeling implication of our study is that a superparameterized GCM or global CRM likely needs very high resolution — on the order of $\Delta x=250\text{m}$ and $\Delta z=100\text{m}$ — to realistically simulate subtropical boundary layer cloud feedbacks on climate. While the required resolution is computationally infeasible for a global CRM for the foreseeable future, it might be within reach of a suitably-designed superparameterized GCM.

Acknowledgments: This work has been supported by the National Science Foundation Science and Technology Center for Multi-Scale Modeling of Atmospheric Processes, managed by Colorado State University under cooperative agreement No. ATM-0425247. The SAM CRM was kindly provided by Marat Khairoutdinov, who also performed the SP-CAM simulations that are the basis for this study.

Appendix A: Vertical velocity feedback equation

As in CB08, we consider a system in which domain-mean anomalies of virtual temperature and diabatic heating in the simulated column are assumed to be representative of a region of characteristic half-width Λ . The resulting horizontal buoyancy gradients generate vertical motions through linear gravity wave dynamics. We modify CB08's derivation (which did not include momentum damping) by allowing a momentum damping rate a_m . For simplicity, we do not consider the advection of anomalies by the reference-state vertical and horizontal winds, which (as shown via scaling analysis in CB08) should not influence the result.

We assume a constant Coriolis parameter f . Our vertical velocity equation is derived assuming the column density anomalies are ‘quasi-steady’, i. e. varying on timescales much longer than a_m^{-1} and f^{-1} , so that we can neglect time-derivative terms in the governing equations. This is not an important restriction, since we run the column model to a statistically steady state.

We consider an arbitrary small perturbation $F^*(x, p, t)$ of all variables F about the reference state F_0 . For simplicity, this perturbation includes variability in only one horizontal dimension, but the same result would also be obtained assuming sinusoidal horizontal variability in two horizontal dimensions. The linear, damped, hydrostatic, quasi-steady momentum and mass conservation equations in pressure coordinates can be written

$$a_m u^* - f v^* = - \frac{\partial \phi^*}{\partial x} \quad (\text{A.1})$$

$$a_m u^* - f u^* = 0 \quad (\text{A.2})$$

$$\frac{\partial \phi^*}{\partial p} = - \frac{R_d T_v^*}{p} \quad (\text{A.3})$$

$$\frac{\partial u^*}{\partial x} + \frac{\partial \omega^*}{\partial p} = 0 \quad (\text{A.4})$$

These equations can be combined into a single equation relating ω^* to the virtual temperature perturbation T_v^* :

$$\frac{\partial}{\partial p} \left(\frac{f^2 + a_m^2}{a_m} \frac{\partial \omega^*}{\partial p} \right) = - \frac{R_d}{p} \frac{\partial^2 T_v^*}{\partial x^2} \quad (\text{A.5})$$

At the surface and the tropopause, we assume rigid-lid boundary conditions and neglect Eulerian pressure tendencies so

$$\omega^*(x, p_s) = \omega^*(x, p_T) = 0 \quad (\text{A.6})$$

We assume the anomalies of all variables F have the spatial structure

$$F^*(x, z, t) = F'(z, t) \cos(kx), \quad (\text{A.7})$$

where $k = \pi/(2\Lambda)$ is a user-specified characteristic horizontal wavenumber. Primes denote the column anomalies from the reference state. Substituting (A.7) into (A.5),

$$\frac{\partial}{\partial p} \left(\frac{f^2 + a_m^2}{a_m} \frac{\partial \omega'}{\partial p} \right) \approx \frac{k^2 R_d}{p} T_v' \quad (\text{A.8})$$

Equation (A.8) can also be interpreted as the steady state limit of equation (7) in Kuang (2008) and was derived independently by Kuang as a means for implementing the weak temperature gradient approximation in a CRM (personal communication), except that here the effect of rotation is included and pressure is used as a vertical coordinate.

In this paper, two assumptions for a_m have been used: the vertically-varying $a_m(p) = 1 \text{ d}^{-1} (p/p_{\text{ref}})$ where $p_{\text{ref}}=1000$ hPa in the bulk of the paper and the vertically-uniform $a_m(p) = 0.5 \text{ d}^{-1}$ in sect. 6.1. Under the assumption that momentum damping is uniform in the vertical, (A.8) becomes:

$$\frac{\partial^2 \omega'}{\partial p^2} \approx r \frac{T_v'}{p} \quad (\text{A.9})$$

where $r = k^2 R_d a_m / (f^2 + a_m^2)$. One can generate an independent estimate of r by comparing LTS-sorted bin-mean profiles of ω' and T_v' in the lower troposphere in SP-CAM, now treating the perturbation as being the difference between the bin-mean and the tropics-wide mean. This results in $r \sim 4.3 \times 10^{-6} \text{ K}^{-1} \text{ s}^{-1}$, which is approximately equivalent to the value r would take on using the choices of k and the vertically-uniform $a_m = 0.5 \text{ d}^{-1}$ above. While the assumption of a vertically-uniform a_m used in the estimate

of r prevents a direct comparison with the default, vertically-varying a_m used in this paper, the estimate of r from SP-CAM also corresponds roughly to the value of the vertically-varying a_m evaluated at 500 hPa. The similarity of this estimate to our choices of a_m and Λ is reassuring, and suggests that the magnitude of vertical velocity feedback we are using is comparable to that apparent in the mean tropical Hadley-Walker circulation in SP-CAM. It also suggests that (2.2) may also be suitable for more idealized frameworks for studying cloud feedbacks such as proposed by Zhang and Bretherton (2008) without large adjustments in a_m and Λ .

Our approach bears some resemblance to Raymond and Zeng's (2005) algorithm for enforcing the weak temperature gradient approximation in a cloud-resolving model. They assumed ω' is proportional to $-a_{\text{wtg}}T_v'$, with a relaxation rate a_{wtg} that goes to zero at the surface and tropopause and maximizes in the mid-troposphere. With an appropriate choice of a_{wtg} , this will have roughly the same effect as (2.2) for gravity waves with a half-wavelength that spans the troposphere, but then it will distort the ω' response to sharper (shorter vertical wavelength) perturbations in T_v in a manner that depends on how far they are from the top or bottom boundary. Unlike Raymond and Zeng's approach, our algorithm (2.2) has the attraction of being formally derivable from a physically-based model of the dynamical feedbacks on horizontally localized density perturbations.

We believe that, for our application, the approach proposed here is superior to that proposed by CB08. While the two approaches start with a similar underlying model of the dynamical adjustment process, CB08 neglected momentum damping. After some approximation, they were ultimately able to relate ω' to the profile of perturbation diabatic heating rate in the simulated column. At least in the lower troposphere, momentum damping is probably quite significant for gravity waves of short vertical wavelength propagating thousands of kilometers across the tropics. For instance, a hydrostatic gravity wave of vertical wavelength 3 km (which projects strongly onto the strong and sharp horizontal temperature variations seen around the trade inversion) has a horizontal phase speed of roughly 5 m s⁻¹. Over the damping timescale $a_m^{-1} \sim 1$ d in the lower troposphere, it will only propagate ~ 500 km, so it experiences considerable momentum damping in the regime half-width $\Lambda = 650$ km. Thus, CB08's neglect of momentum damping was not fully justified for our application. In addition, an approach based on temperature rather than heating rate perturbations has practical advantages when used with a CRM of finite domain size. The CRM-simulated domain-mean heating rate varies much more from time step to time step than does the domain mean temperature, violating the quasi-steady assumption underlying the ω' feedbacks derived by CB08, even while the ω' derived from 2.2 varies only slowly from timestep to timestep. That said, for this study we also tried implementing variants of the

CB08 approach to diagnosing ω' , and with appropriate parameter choices we were able to obtain results quite similar to those shown in this paper (but not shown here due to space limitations).

References

- Abel, S. J., and B. J. Shipway, 2007: A comparison of cloud-resolving model simulations of trade wind cumulus with aircraft observations taken during RICO. *Quart. J. Roy. Meteor. Soc.*, **133**, 781–794, doi: [10.1002/qj.55](https://doi.org/10.1002/qj.55).
- Bony, S., J.-L. Dufresne, H. Le Treut, J.-J. Morcrette, and C. Senior, 2004: On dynamic and thermodynamic components of cloud changes. *Clim. Dyn.*, **22**, 71–86, doi: [10.1007/s00382-003-0369-6](https://doi.org/10.1007/s00382-003-0369-6).
- Caldwell, P., and C. S. Bretherton, 2008: Response of a subtropical stratocumulus-capped mixed layer to climate and aerosol changes. *J. Climate*, **22**, 20–38, doi: [10.1175/2008JCLI1967.1](https://doi.org/10.1175/2008JCLI1967.1).
- Khairoutdinov, M. F., and D. A. Randall, 2001: A Cloud Resolving Model as a Cloud Parameterization in the NCAR Community Climate System Model: Preliminary Results. *Geophys. Res. Lett.*, **28**(18), 36173620, doi: [10.1029/2001GL013552](https://doi.org/10.1029/2001GL013552).
- Khairoutdinov, M. F., and D. A. Randall, 2003: Cloud resolving modeling of the ARM summer 1997 IOP: Model formulation, results, uncertainties, and sensitivities. *J. Atmos. Sci.*, **60**, 607–625, doi: [10.1175/1520-0469\(2003\)060<0607:CRMOTA>2.0.CO;2](https://doi.org/10.1175/1520-0469(2003)060<0607:CRMOTA>2.0.CO;2).
- Kuang, Z., 2008: Modeling the interaction between cumulus convection and linear gravity waves using a limited-domain cloud system-resolving model. *J. Atmos. Sci.*, **65**, 576–591, doi: [10.1175/2007JAS2399.1](https://doi.org/10.1175/2007JAS2399.1).
- Lin, J.-L., M. Zhang, and B. Mapes, 2005: Zonal Momentum Budget of the Madden-Julian Oscillation: The Source and Strength of Equivalent Linear Damping. *J. Atmos. Sci.*, **62**, 2172–2188, doi: [10.1175/JAS3471.1](https://doi.org/10.1175/JAS3471.1).
- Raymond, D. J., and X. Zeng, 2005: Modeling tropical atmospheric convection in the context of the weak temperature gradient approximation. *Quart. J. Roy. Meteor. Soc.*, **131**, 1301–1320, doi: [10.1256/qj.03.97](https://doi.org/10.1256/qj.03.97).
- Siebesma, A. P., and 12 co-authors, 2003: A large eddy simulation intercomparison study of shallow cumulus convection. *J. Atmos. Sci.*, **60**, 1201–1219, doi: [10.1175/1520-0469\(2003\)60<1201:ALESIS>2.0.CO;2](https://doi.org/10.1175/1520-0469(2003)60<1201:ALESIS>2.0.CO;2).
- Sobel, A. H., and C. S. Bretherton, 2000: Modeling Tropical Precipitation in a Single Column. *J. Climate*, **13**, 4378–4392, doi: [10.1175/1520-0442\(2000\)013<4378:MTPIAS>2.0.CO;2](https://doi.org/10.1175/1520-0442(2000)013<4378:MTPIAS>2.0.CO;2).
- Stevens, B., and 16 co-authors, 2005: Evaluation of Large-Eddy Simulations via Observations of Nocturnal Marine Stratocumulus. *Mon. Wea. Review*, **133**, 1443–1462, doi: [10.1175/MWR2930.1](https://doi.org/10.1175/MWR2930.1).
- Stevens, D. E., A. S. Ackerman, and C. S. Bretherton, 2002: Effects of domain size and numerical resolution on the simulation of shallow cumulus convection.

- J. Atmos. Sci.*, **59**, 3285–3301, doi: [10.1175/1520-0469\(2002\)059<3285:EODSAN>2.0.CO;2](https://doi.org/10.1175/1520-0469(2002)059<3285:EODSAN>2.0.CO;2)
- Wyant, M. C., C. S. Bretherton, H. A. Rand, and D. E. Stevens, 1997: Numerical simulations and a conceptual model of the stratocumulus to trade cumulus transition. *J. Atmos. Sci.*, **54**, 168–192, doi: [10.1175/1520-0469\(1997\)054<0168:NSAACM>2.0.CO;2](https://doi.org/10.1175/1520-0469(1997)054<0168:NSAACM>2.0.CO;2)
- Wyant, M. C., Bretherton, C. S., and Blossey, 2009: Subtropical low cloud response to a warmer climate in a superparameterized climate model. Part I: Regime sorting and physical mechanisms. *J. Adv. Mod. Earth Sys.*, **1**, Art. #7, 11 pp., doi: [10.3894/JAMES.2009.1.7](https://doi.org/10.3894/JAMES.2009.1.7).
- Zhang, M., and C. S. Bretherton, 2008: Mechanisms of low cloud-climate feedback in idealized single-column simulations with the Community Atmospheric Model, version 3 (CAM3). *J. Climate*, **21**, 4859–4878, doi: [10.1175/2008JCLI2237.1](https://doi.org/10.1175/2008JCLI2237.1).